

*Dynamic-mechanical response of
carbon fiber laminates with a reactive
thermoplastic resin containing phase
change microcapsules*

**Giulia Fredi, Andrea Dorigato &
Alessandro Pegoretti**

**Mechanics of Time-Dependent
Materials**

An International Journal Devoted to the
Time-Dependent Behaviour of Materials
and Structures

ISSN 1385-2000
Volume 24
Number 3

Mech Time-Depend Mater (2020)
24:395-418
DOI 10.1007/s11043-019-09427-y

Your article is protected by copyright and all rights are held exclusively by Springer Nature B.V.. This e-offprint is for personal use only and shall not be self-archived in electronic repositories. If you wish to self-archive your article, please use the accepted manuscript version for posting on your own website. You may further deposit the accepted manuscript version in any repository, provided it is only made publicly available 12 months after official publication or later and provided acknowledgement is given to the original source of publication and a link is inserted to the published article on Springer's website. The link must be accompanied by the following text: "The final publication is available at link.springer.com".



Dynamic-mechanical response of carbon fiber laminates with a reactive thermoplastic resin containing phase change microcapsules

Giulia Fredi¹ · Andrea Dorigato¹ ·
Alessandro Pegoretti¹

Received: 31 January 2019 / Accepted: 10 September 2019 / Published online: 23 September 2019
© Springer Nature B.V. 2019

Abstract Dynamic-mechanical analysis (DMA) was performed to investigate the viscoelastic response of multifunctional laminates for thermal energy storage (TES). The laminates were constituted by a microencapsulated paraffinic phase change material (PCM), a carbon fiber fabric, and an innovative reactive acrylic resin (Elium[®]). In the Elium[®]/PCM systems, the PCM fraction affected neither the glass transition temperature (T_g) of the resin, found at 100–120 °C, nor the activation energy of the glass transition, determined with multifrequency scans from the position of the $\tan \delta$ peaks. On the other hand, the low-temperature (0–40 °C) transition detected on the neat resin was hidden by the PCM melting, evidenced by a step in E' and peaks in E'' and $\tan \delta$. In the laminates, the amplitude of the E' step and the intensity of the $\tan \delta$ peak associated to the PCM melting presented a linear correlation with the PCM content and the melting enthalpy. Cyclic heating/cooling DMA tests showed that the decrease in E' due to PCM melting was almost completely recovered (90–95%) upon crystallization. The difference between the $\tan \delta$ peak positions on heating and on cooling decreased from 30 to 12 °C when the heating/cooling rate changes from 3 to 1 °C/min. Multifrequency tests highlighted that the activation energy of the glass transition of the laminates was lower than that of the matrices, and it did not follow a trend with the PCM fraction. Interestingly, also the E'' and $\tan \delta$ peaks related to PCM melting depended on the testing frequency, and their asymmetric shape could be interpreted by considering a progressive melting of the PCM in the microcapsules during heating.

Keywords Phase change materials · Thermal energy storage · Paraffin · Dynamic-mechanical analysis · Thermoplastic composites

✉ G. Fredi
giulia.fredi@unitn.it

✉ A. Pegoretti
alessandro.pegoretti@unitn.it

¹ Department of Industrial Engineering, University of Trento, Via Sommarive 9, 38123 Trento, Italy

1 Introduction

Thermal energy storage (TES) is one of the key technologies for a more efficient and rational use of energy resources, as it allows the temporary conservation of excess heat that can be released when the demand for thermal energy overcomes its availability. Such techniques are especially useful to manage intermittent energy sources (e.g., solar) and to recover waste industrial heat (Pielichowska and Pielichowski 2014; Pereira da Cunha and Eames 2016; Zhang et al. 2016). Among the most promising materials for TES are the organic solid–liquid phase change materials (PCMs), which accumulate heat when they melt and release it upon crystallization (Zalba et al. 2003; Sharma et al. 2015). As they can store a high amount of latent heat at a nearly constant temperature, they are often used to maintain the temperature in a specific range; this makes them suitable for thermal management applications, such as to regulate the indoor environment in buildings (Chen et al. 2013; Cao et al. 2014), to avoid overheating of batteries or other electronic devices (Wirtz et al. 2003; Jagemont et al. 2018), or to help maintaining the body temperature constant through smart thermoregulating textiles (Liu and Lou 2015). Among these materials, investigated from the early 1980s (Abhat 1983), paraffin waxes stand out as they are chemically inert, non-corrosive, inexpensive, largely available, and can be found in a wide range of phase change temperatures that depend on the molecular weight (Cao et al. 2014; Sobolciak et al. 2016; Kahwaji et al. 2018; Wang et al. 2019).

As all the solid–liquid PCMs, paraffins must be confined to avoid leakage and loss of material above the melting temperature. In many civil engineering applications, paraffins are stored in tanks or containers (Zalba et al. 2003), but other methods involve the encapsulation in polymeric/inorganic micro/nano-shells (Bayés-García et al. 2010; Hu et al. 2018), or the “shape stabilization” in a nanofiller network that, thanks to the high specific surface area, grasps the PCM polymer chains and prevents leakage (Jeong et al. 2014; Fang et al. 2014; Dorigato et al. 2017a). These two methods are often used in combination with the embedment of PCMs in a polymer matrix. Free, microencapsulated or shape-stabilized paraffins can be blended with many different polymers, and these blends are good candidates to realize smart TES materials that are easily shapeable, lightweight, and relatively inexpensive; they are suitable for storage of thermal energy, indoor thermal comfort in buildings and vehicles, and thermal protection of electronic components, medical items and food (Kenisarin and Mahkamov 2007; Kenisarin and Kenisarina 2012; Sobolciak et al. 2015). The scientific literature reports many examples of such polymer-based, PCM-enhanced materials. The most common polymers that are combined with paraffinic PCMs are polyethylene (Krupa et al. 2014; Zhang et al. 2010; Sobolciak et al. 2016; Dorigato et al. 2017b), polypropylene (Krupa et al. 2007; Mochane and Luyt 2012), polyurethane (Sarier and Onder 2007; Rigotti et al. 2018), and epoxy resin (Wang et al. 2011; Su et al. 2012, 2011; Luyt and Krupa 2009; Jeong et al. 2014). Polyolefins are generally chosen for their high chemical compatibility with paraffins, while epoxies have the advantage of being processed at room temperature, thereby allowing the paraffins to be in the solid state during processing. However, in most cases, the PCM addition decreases the mechanical properties of the host polymer, as these low molecular weight compounds exhibit scarce strength and ductility, and the lack of adhesion between the polymer matrix and the PCM domains (or the microcapsule shell) may lead to premature failure of the polymer component (Wang et al. 2011; Su et al. 2012).

An effective solution to address this problem is the incorporation of reinforcing fibers. Carbon or polymer fibers are the most suitable choice, as their low density allows for a high volume fraction at a relatively low weight fraction, thus preserving the possibility to introduce a high weight concentration of PCM. This would pave the way to produce multifunctional composites combining good mechanical performance and TES capability, useful

where lightness, high mechanical properties, and heat storage/management are equally important (e.g., in automotive, portable electronics). Although the PCM-containing polymers have been well investigated in the literature, very few examples are reported of polymer-matrix composites containing PCMs and reinforcing fibers. Yoo et al. produced and characterized epoxy/glass laminate containing a microencapsulated paraffin (Yoo et al. 2016, 2017a). Our group produced an epoxy/carbon laminate with paraffin shape stabilized with carbon nanotubes (Fredri et al. 2017, 2018a), a polyamide/glass laminate with paraffin microcapsules (Fredri et al. 2018b; Dorigato et al. 2018), short-carbon-fiber composites with a polyamide (Fredri et al. 2019b) or an epoxy (Dorigato et al. 2019) matrix, both containing paraffin microcapsules. This broad-range investigation led to the considerations that carbon fibers allow for a higher fiber volume fraction than glass fibers due to the lower density, and that the high temperatures and shear stresses required to process thermoplastic matrices cause considerable microcapsules breakage. To combine the advantages of the thermoplastics and the mild production process of thermosets, the newly developed reactive methyl-methacrylate-based thermoplastic resin Elium[®] was combined with a carbon fabric and paraffin microcapsules in different weight fractions (Fredri et al. 2019a). The resulting laminates were thermo-mechanically characterized and resulted to be promising candidates for structural TES applications. However, this work lacked a thorough investigation on the dynamic-mechanical properties and the viscoelastic behavior. It is well known that viscoelasticity is an important aspect for the structural performance of polymer composites, and studying the time- and temperature-dependent behavior of a composite is fundamental to understand its mechanical response and long-term performance (Chartoff et al. 2009; Menard 2008). For this aim, dynamic-mechanical analysis (DMA) is a well-established, powerful, and versatile tool to measure the viscoelastic parameters of a polymer composite as a function of time and temperature. It also gives information on the glass transition and other thermally activated transitions, as well as further parameters like the entanglement density, adhesion factor, and reinforcing efficacy of the added fillers. Moreover, it enables the study of the thermomechanical response under a load applied with varying frequency, which allows for a full understanding of the viscoelastic parameters of the investigated polymer (Goertzen and Kessler 2007; Bagotia and Sharma 2019).

DMA is also important for polymers and composites containing a PCM, because its phase transition may alter the mechanical and dynamic-mechanical properties in the service temperature interval around the phase change temperature. Although dynamic-mechanical tests have been performed on some PCM-enhanced polymers (Krupa et al. 2007; Mngomezulu et al. 2010; Sobolciak et al. 2015; Lian et al. 2017; Popelka et al. 2018), the characterization of a PCM-containing laminate through dynamic-mechanical analysis (DMA) can be found in the open literature only once, in the aforementioned work of Yoo et al., dealing with epoxy/glass laminates (Yoo et al. 2017b). However, besides working with a well-known matrix such as epoxy, that research focused on the effect of temperature and frequency on the glass transition of epoxy, and it did not analyze carefully the behavior of the viscoelastic parameters around the PCM phase change temperature. Moreover, that work concentrated only on the laminates, without studying the effect of the microcapsules on the sole matrix.

The present work aims at providing, for the first time, a detailed investigation of the dynamic-mechanical behavior of Elium[®]/PCM systems and Elium[®]/PCM/carbon fiber laminates, to understand how the PCM addition affects the viscoelastic parameters and the glass transition of the host matrix or laminate, and how they change before, during, and after the PCM phase change. The analysis was performed with different testing modes, i.e., single frequency scans, multifrequency analysis, and heating/cooling cycles. Moreover, this study aims at assessing the suitability of the DMA techniques to study a melting/crystallization phase transition, which is an unusual application for this analysis.

2 Materials and method

The materials and sample preparation, concisely reported hereafter, have been described in detail in a previous paper of our group (Fredri et al. 2019a).

2.1 Materials

The reactive thermoplastic methyl-methacrylate-based resin Elium[®] 150 was kindly provided by Arkema (Lacq, France). The polymerization initiator, supplied with the resin by the producer, was anhydrous benzoyl peroxide (BPO) with 50% active content. The PCM was the Microtek[®] MPCM43D, obtained by Microtek Laboratories Inc. (Dayton, OH, USA); it is constituted by microcapsules in which the core phase change material is a paraffin wax (melting point 43 °C) and the shell is melamine-formaldehyde-based. As reported on the product datasheet, the average capsule diameter is 20 µm, and the phase change enthalpy is 190–200 J/g. The balanced, plain-weave carbon fiber fabric GG200P was acquired from G. Angeloni S.r.l. (Venice, Italy), and it has a mass per unit area of 192 g/m². All the materials were used as received.

2.2 Sample preparation

Elium[®] and BPO (98:2 wt:wt) were manually mixed until complete dissolution of BPO. The paraffin microcapsules (MC) were then added in concentrations of 20, 30, and 40 wt%. The mixtures were subsequently mechanically stirred, degassed, poured in silicon molds, left 4 hours at room temperature, and thermally treated for 8 hours at 80 °C. Neat resin samples were also prepared for comparison. The same four compositions were also used as matrices to produce 5-ply laminates having an in-plane area of 13 × 20 mm². The laminates were obtained through hand layup and vacuum bag techniques and thermally treated in the same way as the matrices. As thoroughly described in Fredri et al. (2019a), the sample preparation led to a non-negligible evaporation of the most volatile fraction of the resin, thereby causing an increase in the final MC:resin ratio. However, all the samples have been conveniently named after the nominal (initial) MC weight fraction in the matrix. The nominal and experimental compositions of the prepared matrices and laminates are reported in Table 1. It can be noticed that the fiber fraction in the laminates decreases with an increase in the MC loading. This is related to the rise in the matrix viscosity with the MC content, which hinders its flowing out of the fabric during the vacuum bag process and leads to a higher matrix weight fraction, as was confirmed by thermogravimetric analysis (TGA). This was also the cause of the higher laminate thickness at elevated MC amounts.

2.3 Characterization

2.3.1 Characterization of the matrices

The microstructure was investigated through a field emission scanning electron microscope (FE-SEM) Zeiss Supra 60, after liquid N₂ cryofracturing and Pt–Pd sputtering.

Differential scanning calorimetry (DSC) was carried out with a Mettler DSC30 instrument; heating–cooling–heating tests were performed on samples of approx. 20 mg, in the temperature interval 0–130 °C, at the scanning speed of 10 °C/min. A DSC test at 1 °C/min was also performed on neat MC to study the phase change transition in more detail. The test

Table 1 List of the prepared samples with the experimental compositions

Matrices	EL	EL-MC20	EL-MC30	EL-MC40
MC (wt %)	0	25.3 ± 0.6	36.9 ± 1.2	48.0 ± 0.4
Laminates	EL-CF	EL-MC20-CF	EL-MC30-CF	EL-MC40-CF
MC (wt%)	0	14.5	22.1	32.1
CF (wt%)	66.9 ± 1.4	48.1 ± 0.3	38.9 ± 2.6	38.2 ± 1.8
CF (vol%)	56.7 ± 1.6	35.6 ± 0.6	27.4 ± 1.9	25.0 ± 1.2
Porosity (vol%)	1.6 ± 2.1	2.2 ± 1.3	1.2 ± 3.2	5.2 ± 2.4
<i>t</i> (mm)	1.12	1.42	2.00	2.30

MC = microcapsules; CF = carbon fibers; *t* = laminate thickness

led to the determination of the melting/crystallization temperatures (T_m , T_c) and enthalpies (ΔH_m , ΔH_c) of the PCM, as well as the glass transition temperature of the resin (T_g).

Dynamic-mechanical analysis (DMA) was performed with a TA Q800DMA instrument in single cantilever bending mode (span = 17.5 mm), on specimens of $35 \times 10 \times 3$ mm³. Storage modulus (E'), loss modulus (E''), and loss factor ($\tan\delta$) were measured in the temperature interval 0–160 °C, at a heating rate of 3 °C/min, at a strain amplitude of 0.05% and a frequency of 1 Hz. Multifrequency scans were also carried out on samples of the same geometry. The tests were performed at 0.3 mm/min at the frequency levels 0.3, 1, 3, 10, and 30 Hz. The activation energy of the glass transition (E_a) was determined through the Arrhenius approach, from the slope of the linear regression of the natural logarithm of the applied frequency plotted versus the reverse of the $\tan\delta$ peak temperatures, as reported in Eq. (1):

$$E_a = R \left[\frac{d(\ln \nu)}{d(1/T_p)} \right] \quad (1)$$

where R is the universal gas constant, equal to 8.314 J/mol K, ν is the applied frequency, and T_p is the E'' or $\tan\delta$ peak temperature at the glass transition.

2.3.2 Characterization of the laminates

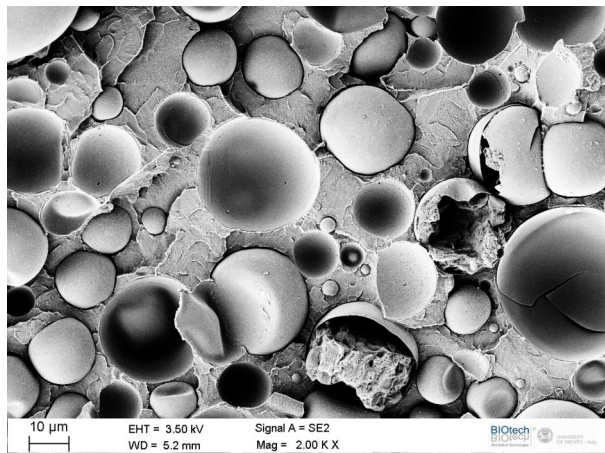
Optical microscope (OM) images of the polished cross-sections were acquired with an up-right incident-light optical microscope Zeiss Axiophot equipped with Epiplan Neofluar objectives.

Single frequency and multifrequency DMA tests were performed as described for the matrices, on samples with nominal in-plane area of 35×5 mm² (and the thickness of each laminate, see Table 1).

Additionally, cyclic DMA scans were performed to assess the recovery of E' and the behavior of other viscoelastic parameters upon PCM crystallization. Heating–cooling–heating scans were performed between –40 and 60 °C, at the scanning speeds of 3 and 1 °C/min. The test allowed the measurement of all the peak temperatures of E'' and $\tan\delta$, the ratio between the values of E' at the beginning of the second and the first heating scans ($E'_{rel,-40\text{ }^\circ\text{C}}$), and the temperature difference at the middle value of E' between the first heating scan (h_1) and the cooling scan (c), defined through Eq. (2) as

$$\Delta T_{E',50\%} = T(E'_{50\%,h_1}) - T(E'_{50\%,c}) \quad (2)$$

Fig. 1 SEM micrograph of the cryofracture surface of the sample EL-MC30



where $E'_{50\%}$ is the average between the maximum and the minimum E' values of each sample.

3 Results and discussion

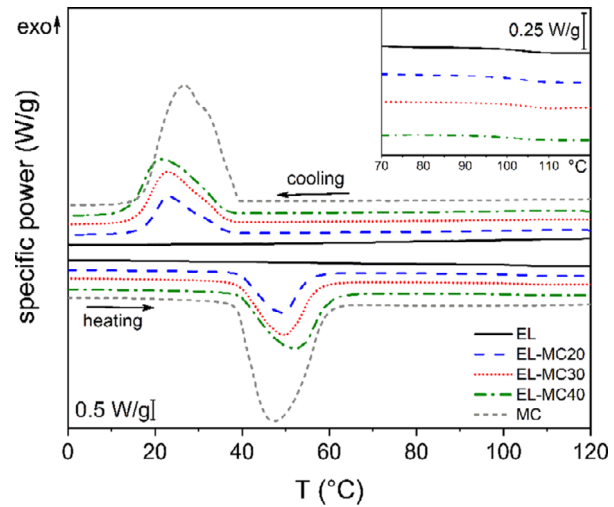
3.1 Characterization of the matrices

Studying the effect of PCM introduction in a reactive acrylic matrix is useful not only because it allows for a better understanding of the mechanical and viscoelastic properties of the Elium[®]-based laminates, but also because such PCM-enhanced in-situ polymerizing acrylic formulations are being developed *per se* as smart bone cements, in which the PCM absorbs the excess heat developed during polymerization and prevents bone necrosis (Lv et al. 2015). Their mechanical and viscoelastic properties are thus worth to be investigated.

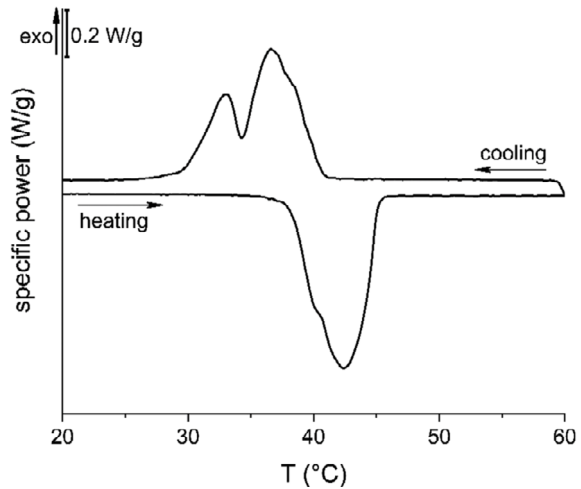
Figure 1 reports an example SEM micrograph of the cryofracture surface of the sample EL-MC30 at a magnification of 2kx. The capsules appear homogeneously distributed in the matrix. It can be observed that some capsules are broken, which is likely due to the cryofracturing stage and not as a consequence of the rather mild processing conditions. The damaged capsules evidence the core-shell structure of this PCM, with a smooth shell and an irregular-shaped paraffinic core. The presence of numerous broken capsules implies a rather good capsule–matrix adhesion, as the fracture propagates across the capsules and not only at the interface. Nevertheless, some capsules present a noticeable gap at the interface with the matrix, which suggests that the adhesion could be still improved. A more detailed discussion on the SEM results and a presentation of different compositions and more magnification levels are reported in our previous article (Fredri et al. 2019a).

Figure 2(a) shows the DSC scans of the samples EL, EL-MC x ($x = 20, 30, 40$) and MC, and reports the first heating scan and the cooling scan, while the most important DSC results are reported in Table 2. The neat resin (EL) undergoes glass transition (T_g) at 103.6 °C, which is only slightly appreciable from Fig. 2(a). As seen from the data of the samples EL-MC x , ($x = 20, 30, 40$), the presence of MC does not substantially modify the T_g , which implies that the MC does not heavily affect the polymerization process of the resin. However, the T_g signal is quite weak, especially in the samples with a high MC content, and this interferes with a precise identification of the T_g . The neat MC shows an endothermic peak

Fig. 2 (a) DSC thermograms of the samples MC, EL and EL-MC x ($x = 20, 30, 40$) at 10 °C/min. The inset represents the temperature interval around the glass transition in the heating scan; (b) DSC thermogram of the neat MC at 1 °C/min



(a)



(b)

at 45.0 °C in the heating scan, corresponding to paraffin melting, while the crystallization is denoted by an intense exothermic peak in the cooling scan (peak temperature = 29.8 °C). The measured phase change enthalpy on the neat MC was 208.2 J/g, both on heating and on cooling. The same two peaks are evident also for the samples EL-MC x ($x = 20, 30, 40$). The peak intensity increases with an increase in MC content, as also evidenced by the melting enthalpy values (ΔH_m), which are proportional to the MC weight fraction (Table 2). Moreover, the melting temperature (T_m) of all the samples is higher than that of the neat MC, probably due to inertial phenomena. Likewise, the crystallization is shifted to lower temperatures. The detailed values of crystallization temperature and enthalpy, as well as a more exhaustive discussion on the DSC results, are reported in our previous article (Fredri et al. 2019a). Both the endothermic and the exothermic DSC signals of the MC sample (Fig. 2(a)) are the result of the partial superposition of at least two peaks, which can be better appre-

Table 2 Results of DSC and DMA tests on the samples EL and EL-MC x ($x = 20, 30, 40$)

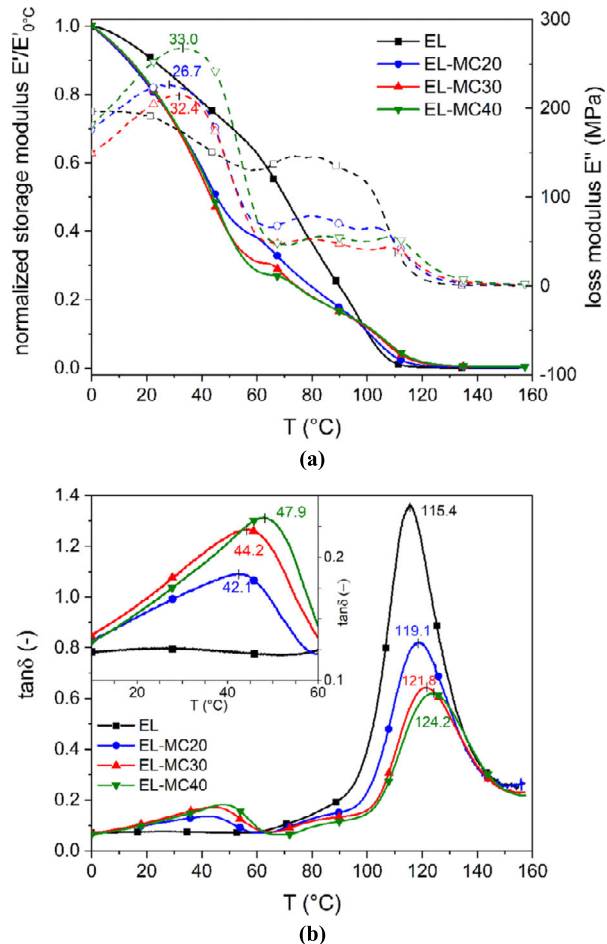
Property	EL	EL-MC20	EL-MC30	EL-MC40
T_g (°C)	103.6	103.8	104.6	101.7
T_m (°C)	–	47.0	47.7	49.9
ΔH_m (J/g)	–	53.1	80.8	101.4
$E'_{60\text{ }^\circ\text{C}}/E'_{0\text{ }^\circ\text{C}}$ (%)	62.7	38.2	31.1	28.4
E'_r (MPa)	1.71	5.49	8.37	10.03
E_a (kJ/mol)	365 ± 12	349 ± 11	348 ± 9	365 ± 7
R^2	0.997	0.996	0.998	0.999

T_g = glass transition temperature from DSC; T_m = melting temperature from DSC; ΔH_m = melting enthalpy from DSC; $E'_{60\text{ }^\circ\text{C}}/E'_{0\text{ }^\circ\text{C}}$ = ratio between the values of E' at the indicated temperatures; E'_r = residual storage modulus after T_g ; E_a = activation energy of the glass transition, calculated from the $\tan \delta$ peaks; R^2 = value of R^2 from the linear regression

ciated from the thermogram acquired at 1 °C/min (Fig. 2(b)), as the lower heating/cooling rate allows for a better signal resolution and a separation of peaks associated to different transitions. The heating scan shows two peaks: the first, at lower temperature, is probably due to the solid–solid transition from the crystalline phase to a less ordered stage called the “rotator phase”, while the second is the result of the solid–liquid phase change, in good agreement with the thorough investigation performed by Wang et al. on the phase change behavior of *n*-docosane (Wang et al. 2003). The cooling scan shows a peak with a shoulder and another smaller asymmetric peak at lower temperature. Three distinct peaks are evident on DSC thermograms performed at an even lower scanning speed (0.2 °C/min), not reported here for the sake of brevity. This evidences multiple transitions and crystalline phases also in the cooling scan, as confirmed by other studies on alkanes crystallization (Dirand et al. 2002; Wang et al. 2003; Vélez et al. 2015; Peng et al. 2018). However, since the paraffinic PCM of the present work is a commercial alkane mixture, it is difficult to precisely attribute each peak to the corresponding transition (Peng et al. 2018). The same multiple peaks have been observed also in the EL-MC x samples tested at 0.2 °C/min (not reported), which highlights that the phase change mechanism of the PCM remains unchanged when embedded in the resin.

The thermal transitions of the MC and the resin were further studied through DMA. Figure 3(a)–(b) reports the trends of E' , E'' , and $\tan \delta$ as functions of the temperature in single frequency scans. The values of E' were normalized to the value at 0 °C for an easier comparison of the samples. The E' of the neat EL shows a general decreasing trend with increasing temperature, but the decrease is more evident at 80–100 °C, in proximity of the glass transition. In that region, E'' shows a broad peak in which two contributions can be evidenced, and the $\tan \delta$ signal presents a single relatively sharp peak at 115.4 °C, with a small left shoulder. The same signals related to the T_g are also present in all the EL-MC x ($x = 20, 30, 40$) samples. The peaks of E'' and $\tan \delta$ at the glass transition are slightly shifted to higher temperature, and this is more evident as the MC content increases. Due to the signal shape, it is easier to observe this phenomenon on the $\tan \delta$ trends, whose peak temperatures are reported directly on the thermograms. This peak shift could be related to the immobilization on the polymer chains at the filler surface; according to the literature, this happens up to a certain filler concentration, beyond which the fillers cause polymer chain separation and increase the segmental motion, as reported for other polymers containing microfillers (Sun

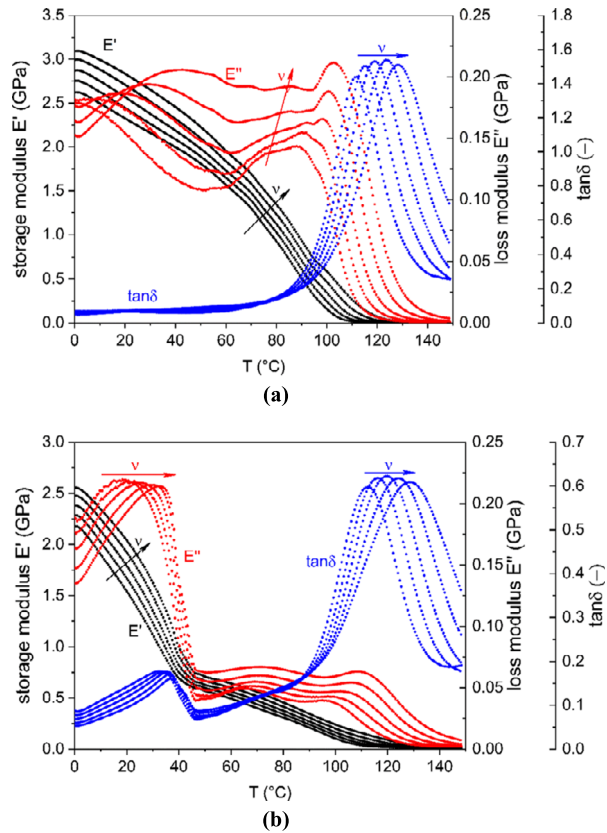
Fig. 3 DMA thermograms of the samples EL and EL-MC x ($x = 20, 30, 40$): **(a)** normalized storage modulus $E'/E'_{0^\circ\text{C}}$ (solid lines) and loss modulus E'' (dashed lines); **(b)** loss tangent $\tan\delta$. The reported values represent the peak temperatures



et al. 2004; Yung et al. 2009; Yoo et al. 2017b). This increase was also observed in DSC, but to a lesser extent and only up to the sample EL-MC30, probably because the weak T_g signal of the sample EL-MC40 hinders an accurate data analysis. In any case, the T_g is only slightly affected by the presence of the PCM, which indicates that the microcapsules do not interfere with the in-situ polymerization of the resin and the introduction of a PCM in the microencapsulated form is a good way to preserve the thermal properties of the resin. This is not the case for other reported polymer matrices containing a shape-stabilized PCM, in which the PCM domains influence the chain mobility and the T_g values (Lian et al. 2017; Sundararajan et al. 2018).

The DMA thermograms of the MC-containing samples show additional signals at the PCM phase transition. The storage modulus decreases markedly in the temperature interval 40–60 $^\circ\text{C}$, and this effect is increasingly evident with increasing MC concentration, as also observable from the data of the normalized E' values at 60 $^\circ\text{C}$ reported in Table 2. On the other hand, in the same temperature interval, evident peaks can be observed on the loss modulus and $\tan\delta$ signals. From a comparison between DMA and DSC thermograms, it can be observed that in DMA the effect of the PCM melting affects the E'' and $\tan\delta$ signals at

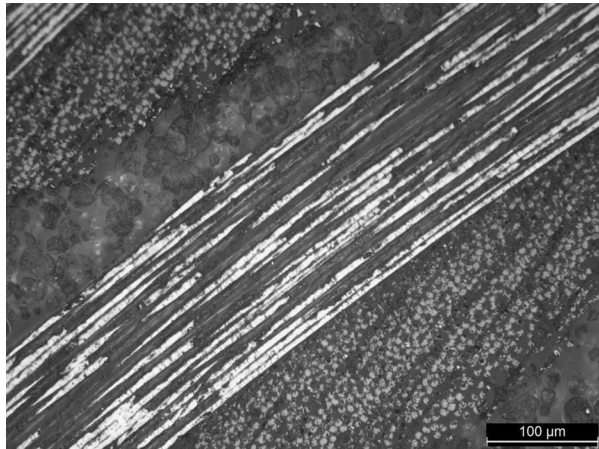
Fig. 4 Results of the DMA multifrequency scans on the samples EL (a) and EL-MC40 (b). Investigated frequencies were 0.3, 1, 3, 10 and 30 Hz



temperatures lower than the DSC melting range. The E'' and $\tan\delta$ onset and peak temperatures are considerably lower than those measured in DSC. Moreover, with an increase in the MC fraction, the E'' peak positions slightly shift to higher temperatures, as observed for DSC, but the peak height does not follow a trend with the MC loading. Similarly, the $\tan\delta$ signals show asymmetric peaks at the PCM melting, and the peak temperatures are closer to those measured in DSC. The peaks move to higher temperatures with increasing MC content and, interestingly, also the peak height increases with the MC fraction, as reported for other PCM-containing polymers (Krupa et al. 2007; Popelka et al. 2018). It is worth mentioning that also the residual storage modulus E'_R at 160 °C, reported in Table 2, increases with increasing MC fraction, which could be still due to the constraint effect of the MC on the polymer chains, as reported for other thermoplastic polymer composites (Gamon et al. 2013).

Multifrequency DMA scans were performed to investigate the effect of the frequency on the PCM melting and the glass transition of the resin. Representative multifrequency thermograms of the samples EL and EL-MC40 are reported in Fig. 4(a)–(b). While increasing the applied frequency, the storage modulus of the neat resin shifts to higher temperatures (Fig. 4(a)). It can be observed that E' depends considerably on the applied frequency not only at the glass transition, but also at lower temperatures, where the broad bands of E'' suggest the presence of an additional low-temperature transition. Similarly, as expected, the E'' and $\tan\delta$ signals are shifted to higher temperatures with increasing frequency, but the $\tan\delta$

Fig. 5 Optical microscope image of the polished cross-section of the laminate EL-MC30-CF



trend shows a strong dependency on the applied frequency only near the T_g . These trends are observable also in the multifrequency scan on the sample EL-MC40 (Fig. 4(b)), where also the E'' and $\tan \delta$ peaks related to the PCM melting (10–40 °C) appear to be influenced by the applied frequency. Unlike the peaks at T_g , the frequency dependence of the melting peaks is more evident before their maximum values than after. This asymmetric behaviour could be attributed to the gradual paraffin melting, which leads to a system with a complex thermo-viscoelastic behaviour.

Multifrequency scans were also performed to estimate the activation energy (E_a) of the glass transition relaxation, i.e., the energy barrier that must be overcome to activate the molecular motions at the basis of the transition (Goertzen and Kessler 2007; Menard 2008). Even though the inflection point of E' and the peak of E'' are normally regarded as more conservative indicators of the T_g (Li et al. 2000), also the $\tan \delta$ signal has been largely used in the literature to determine E_a (Clarke and Braden 1989; Fambri et al. 2003; Karbhari and Wang 2004; Keller et al. 2013). In the present work, E_a was calculated with the peak positions of $\tan \delta$, because the signal is clearer and the peaks sharper than those of E'' , thereby easing the identification of the peak maximum and decreasing the probability of errors related to data analysis. The peak maxima have been used to determine E_a through the standard Arrhenius approach. The values of E_a , reported in Table 2, do not follow a trend with the MC content and the differences among the samples are not significant, which suggests that no substantial structural changes happen in the acrylic matrix upon MC addition.

3.2 Characterization of the laminates

Figure 5 reports an exemplificative optical micrograph of the polished cross-section of the laminate EL-MC30-CF. The microcapsules are preferentially distributed in the interlaminar regions, and not within the fibers of the same yarn. This is due to the difference in size between MC and fibers, which prevents the MC to migrate inside the single yarns during impregnation, and it is part of the reason for the decrease in interlaminar strength and failure properties measured in three-point bending tests (Fredri et al. 2019a).

The DSC thermograms of the laminates are reported in Fig. 6, while the most important DSC results are summarized in Table 3. As for the matrices, the T_g is not considerably affected by the MC, and it is found in the same temperature range as that of the EL-MC x samples, even though at slightly lower values.

Fig. 6 DSC thermograms of the samples EL-CF and EL-MC x -CF ($x = 20, 30, 40$). The first heating scan and the cooling scan are reported

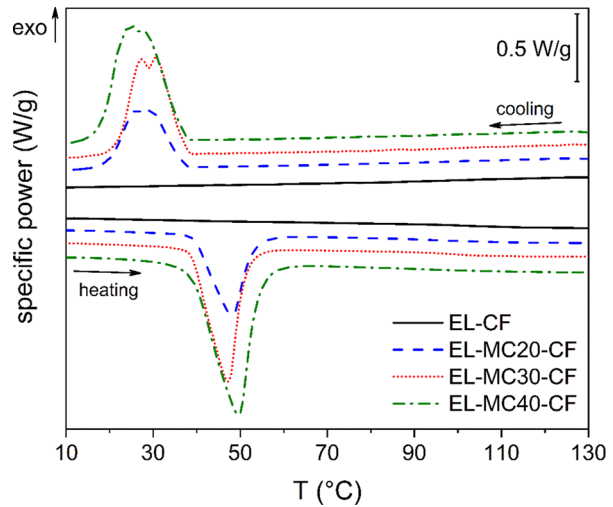


Table 3 Results of the DSC and DMA tests on the samples EL-CF and EL-MC x -CF ($x = 20, 30, 40$)

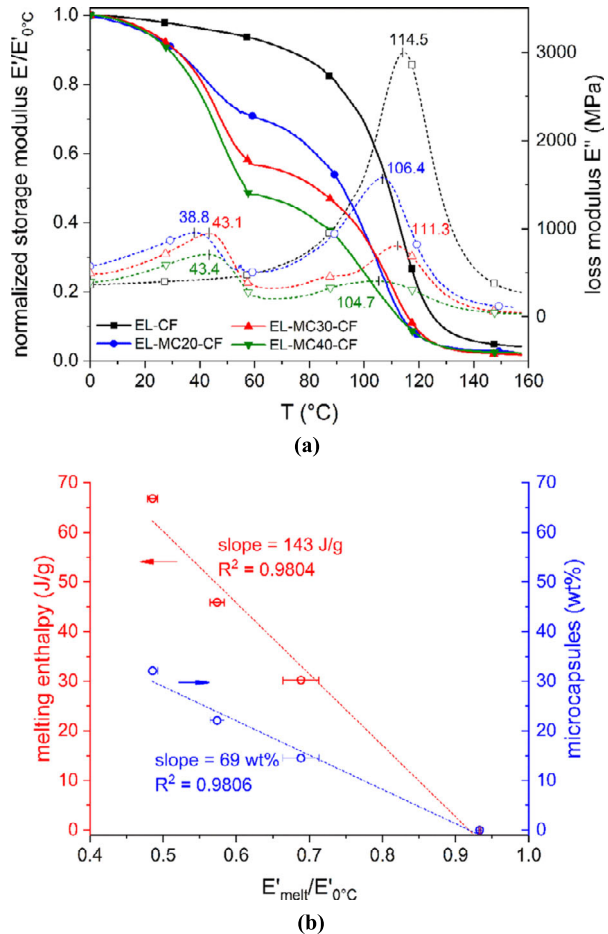
Sample	EL-CF	EL-MC20-CF	EL-MC30-CF	EL-MC40-CF
T_g (°C)	101.0	102.9	99.6	98.6
T_m (°C)	–	46.6	45.3	46.4
ΔH_m (J/g)	–	30.2	45.9	66.8
E_a (kJ/mol)	328 ± 12	320 ± 4	339 ± 8	341 ± 14
$R^2_{\tan \delta}$	0.995	0.999	0.998	0.995

T_g = glass transition temperature from DSC; T_m = melting temperature from DSC; ΔH_m = melting enthalpy from DSC; E_a = activation energy of the glass transition, calculated from the $\tan \delta$ peaks; R^2 = value of R^2 of the linear regression

The values of T_m of the paraffin phase do not change considerably with the MC content, but they are generally lower than those measured on the matrices, which is probably the result of the rise in thermal conductivity due to carbon fiber introduction. This is also supported by the finding that the crystallization temperatures (not reported here) are slightly higher than those of the EL-MC x samples. The phase change enthalpy increases with the MC weight fraction, which implies that the processing of the laminates is sufficiently mild to preserve the MC integrity. As for the samples EL-MC x ($x = 20, 30, 40$), a more detailed discussion on OM, SEM and DSC results of the laminates is presented in our previous article (Fredi et al. 2019a).

As for the matrices, also the laminates underwent a thorough DMA characterization. They were first subjected to single frequency DMA tests, and the results of this investigation are reported in Fig. 7(a)–(d). The values of E' are normalized to the value at 0 °C for an easier comparison of the samples. The storage modulus of the neat EL-CF laminate decreases with increasing temperature throughout the whole temperature range, but the decrease far below T_g is remarkably less evident than for the unfilled EL sample. Moreover, E'' does not present intense peaks in the temperature interval 0–40 °C, which suggests that the low-temperature transition of the acrylic resin may be hindered by the constrains im-

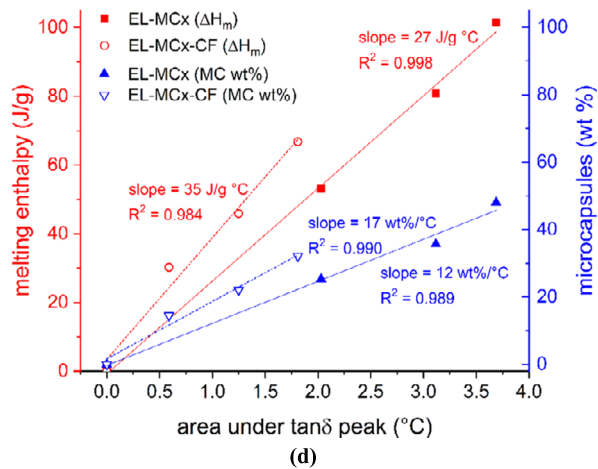
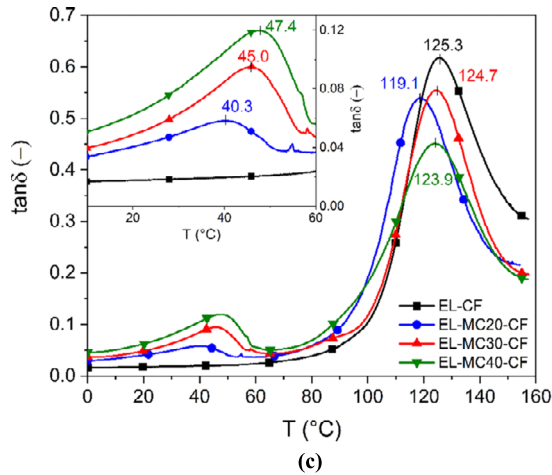
Fig. 7 DMA results of the samples EL-CF and EL-MC x -CF ($x = 20, 30, 40$). The reported values represent the peak temperatures: (a) normalized storage modulus E' (solid lines) and loss modulus E'' (dashed lines); (b) relative decrease in E' after PCM melting (60 °C) as a function of the melting enthalpy and the microcapsules weight fraction; (c) loss tangent $\tan \delta$; (d) area under the $\tan \delta$ melting peak as a function of the melting enthalpy and the microcapsules weight fraction, for the samples EL-MC x and EL-MC x -CF ($x = 20, 30, 40$)



posed by the fibers. Another possible explanation is related to the strong exothermicity of the polymerization of acrylic resins such as Elium (Shin et al. 2019). In the composite, the local temperature can be different from that of the unfilled Elium due to the presence of conducting carbon fibers, and this may affect the DMA behavior. However, further investigation is needed to prove any hypotheses.

On the other hand, the peaks of E'' and $\tan \delta$ at the glass transitions are still evident. In the PCM-containing laminates, E' decreases in two main steps, similarly to the behavior of the matrices; the first step is due to the PCM melting, while the second is associated to the glass transition of the resin. The amplitude of the first step increases with increasing MC fraction. Interestingly, as reported in Fig. 7(b), it shows a linear correlation both with the MC weight fraction and with the phase change enthalpy, with R^2 values higher than 0.98. This suggests that, with a quick test such as the DSC, one can have important information to predict, to a certain extent, the trend of the viscoelastic properties of the composite in the PCM phase change temperature range. The signals of E'' and $\tan \delta$ show peaks at the PCM melting; in this case, the peaks of E'' appear strongly asymmetrical and are qualitatively similar to those of $\tan \delta$. This was not the case for the matrices, probably because of the not negligible contribution of the low-temperature transition of the resin, not appreciable for the

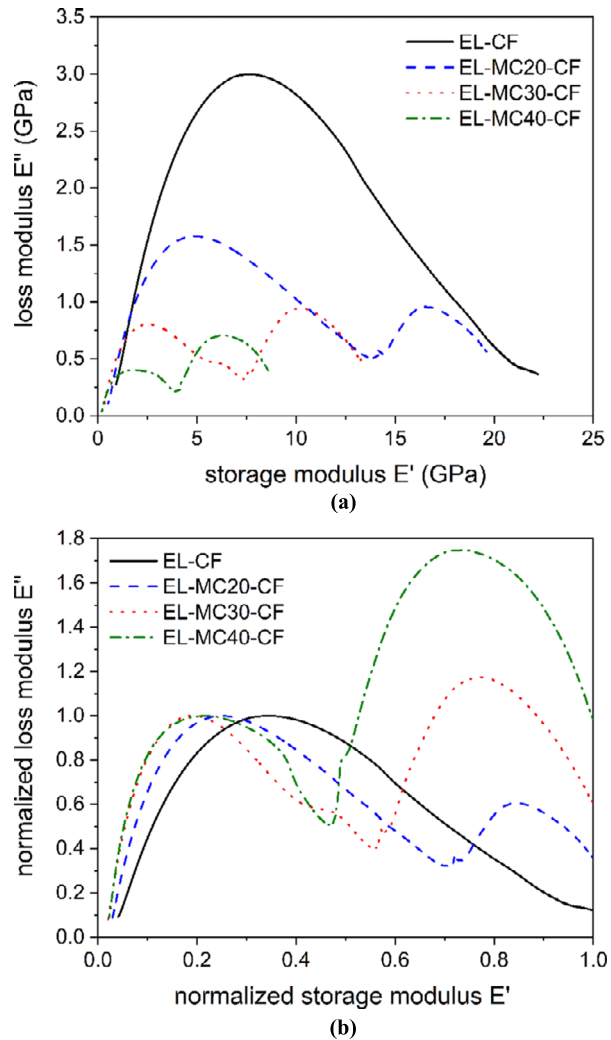
Fig. 7 (Continued)



laminates. However, as for the matrices, the melting peaks shift to higher temperatures and the intensity of the $\tan \delta$ peaks increase with increasing MC content. Interestingly, also the area under the $\tan \delta$ peak shows a quite good linear correlation with the MC weight fraction and the phase change enthalpy. This effect, found also for the matrices, is shown for both classes of samples in Fig. 7(d). The slopes of these trends are lower for the matrices than for the laminates, that is for a fixed value of melting enthalpy (or MC fraction), the intensity of the $\tan \delta$ peak is higher for the matrices than for the laminates.

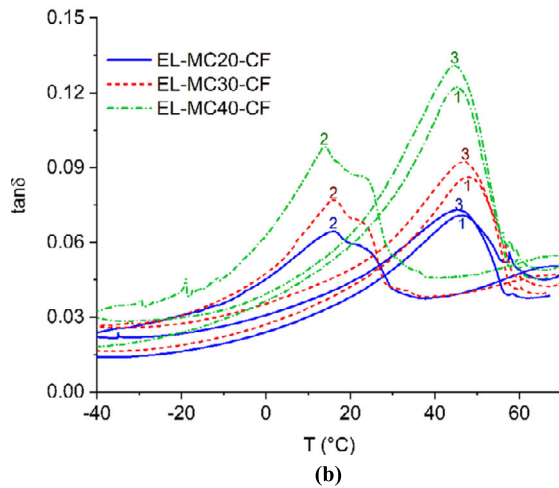
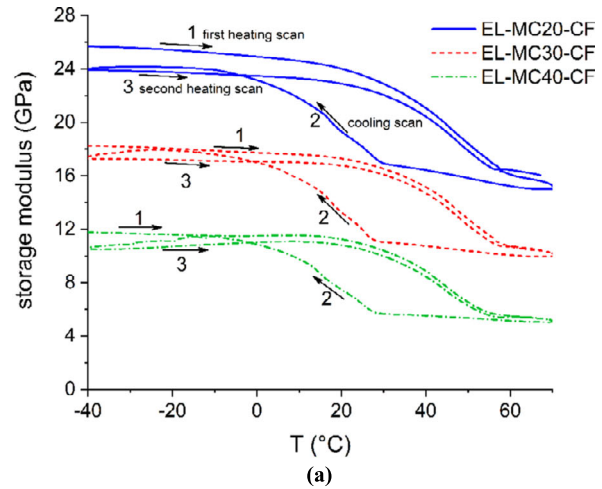
The viscoelastic parameters E' and E'' can also be represented on the Cole–Cole plot, where E'' is plotted as a function of E' on linear axes. This representation has been reported to provide information on the system heterogeneity, secondary relaxations and structural changes after filler addition (Flores et al. 1996; Devi et al. 2009), as well as to assess whether a material can be treated as thermorheologically simple (Menard 2008). Homogeneous polymeric systems with well dispersed fillers exhibit semicircular curves, while heterogeneous multiphase systems present imperfect or elliptical curves (Chee et al. 2019). The Cole–Cole plots of the prepared laminates are presented in Fig. 8(a). The neat EL–CF laminate shows an imperfect semicircle, similar to those reported for another Elium[®]/carbon laminate (Bhudo-

Fig. 8 (a) Cole–Cole plots and (b) normalized Cole–Cole Plots of the DMA single frequency scans on the samples EL-CF and EL-MC x -CF ($x = 20, 30, 40$). The normalization was done by dividing E' values by the initial E' value at 0 °C, and E'' values by the peak of E'' at T_g



lia et al. 2017) and regarded as indicative of a good fiber–matrix adhesion (Chee et al. 2019; Bagotia and Sharma 2019). In the laminates containing MC, the E'' – E' data are distributed on a smaller range in both axes, as the initial values of E' and E'' decrease with increasing MC. The decrease in E' is an indication of the decrease in the stiffness of the laminates with increasing MC content. This effect, observed also in three-point bending tests (Fredri et al. 2019a), is mostly due to the decreasing fiber volume fraction. The Cole–Cole plots of these laminates present two subsequent imperfect semicircles, representative of the two thermal transitions (i.e., PCM melting and resin glass transition). The semicircles related to the glass transition, on the left of the plot, become smaller with increasing MC fraction, and their shape also changes, as better observable from the normalized Cole–Cole plots (Fig. 8(b)). It is interesting to note that also the melting phase transition appears in these plots as imperfect semicircles, which are qualitatively similar for the different compositions and shifted to lower values of E' and E'' with increasing MC concentration. As observable in Fig. 8(b), the

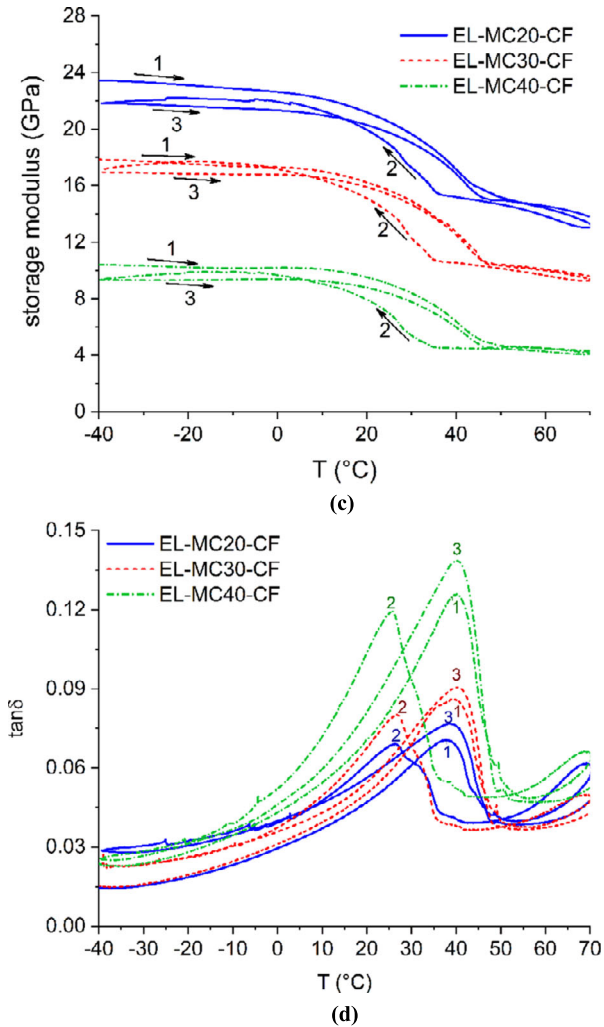
Fig. 9 DMA heating (1)—cooling (2)—heating (3) scans on the samples EL-MC x -CF ($x = 20, 30, 40$) in the temperature range around the phase change temperature of the PCM, at different heating rates: (a) storage modulus at 3 °C/min; (b) $\tan \delta$ at 3 °C/min; (c) storage modulus at 1 °C/min; (d) $\tan \delta$ at 1 °C/min



relative breadth (E' range) and height (E'' range) of the glass transition and melting peaks change significantly with the composition, as the melting peak becomes increasingly higher and broader than the glass transition peak with increasing MC concentration.

As the operating temperature of structural TES composites is around the PCM melting point, these materials must withstand repeated thermal cycles in this temperature range. For this reason, the variation of the viscoelastic parameters was investigated through DMA analysis not only on heating, but also on cooling. This is not a common approach in the field of polymer composites: to the best of the authors' knowledge, no other studies are reported that show the trend of viscoelastic parameters of polymers containing a PCM on cooling. The results of this analysis on the materials object of this work are reported in Fig. 9(a)–(d) and Table 4. Figure 9(a) shows the trend of E' for the PCM-containing laminates, in a heating–cooling–heating scan performed at 3 °C/min. As observed before, E' decreases with increasing MC concentration, and during the first heating scan E' decreases at the PCM melting, but during the cooling scan, this decrease is almost completely recovered. As observed in DSC tests, the crystallization happens at lower temperatures than the melting,

Fig. 9 (Continued)



for reasons related both to thermal inertia and to the thermodynamics of crystallization. The temperature interval describing this delay during the cyclic DMA tests, calculated at the middle value of E' of each sample, is reported in Table 4 as $\Delta T_{E'50\%}$, and it is approx. 26–28 °C. At the end of the cooling scan, E' is almost completely recovered, as it reaches 90–95% of the initial value (Table 4). The trend of $\tan \delta$, reported in Fig. 9(b), shows the same effects: the crystallization peak is found at lower temperatures than the melting peak (approx. 30 °C lower, as reported in Table 4), and the peak in the second heating scan is slightly shifted to higher values than that in the first, but not to higher temperature. The trends of E'' , not reported for the sake of brevity, are qualitatively similar to those of $\tan \delta$. It is interesting to note that two distinct peaks can be detected in the $\tan \delta$ signal on cooling, which reflect the shape of the exothermic peak in DSC. This suggests that the liquid–solid and solid–solid thermal transitions of the PCM can be detected also in DMA, and that each of them brings a contribution to E' and $\tan \delta$.

Table 4 Results of the heating/cooling cycles performed with DMA tests

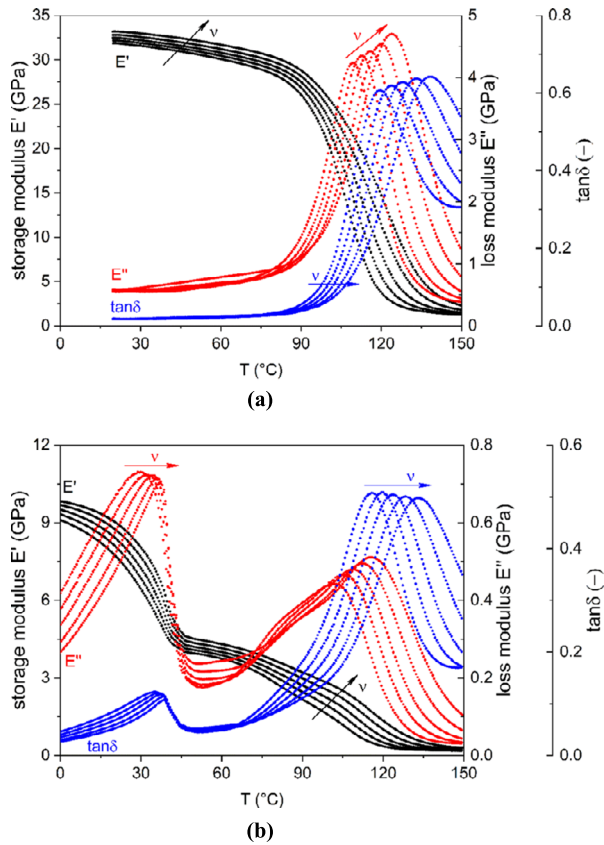
	3 °C/min	EL-MC20-CF	EL-MC30-CF	EL-MC40-CF
$\Delta T_{E'/50\%}$ (°C)	26.7	28.0	26.2	
$E'_{rel,-40^\circ\text{C}}$ (%)	93.3	94.8	89.4	
$T_{h_1,\tan\delta}$ (°C)	46.6	47.5	45.1	
$T_{c,\tan\delta}$ (°C)	16.0	16.1	13.7	
$T_{h_2,\tan\delta}$ (°C)	45.5	46.6	44.4	
$T_{h_2,\tan\delta}-T_{c,\tan\delta}$ (°C)	29.5	30.5	30.7	
1 °C/min	EL-MC20-CF	EL-MC30-CF	EL-MC40-CF	
$\Delta T_{E'/50\%}$ (°C)	9.6	10.7	12.7	
$E'_{rel,-40^\circ\text{C}}$ (%)	93.1	95.0	89.6	
$T_{h_1,\tan\delta}$ (°C)	38.0	39.1	40.2	
$T_{c,\tan\delta}$ (°C)	26.1	26.8	25.7	
$T_{h_2,\tan\delta}$ (°C)	38.5	40.3	40.1	
$T_{h_2,\tan\delta}-T_{c,\tan\delta}$ (°C)	12.4	13.5	14.4	

$\Delta T_{E'/50\%}$ = temperature interval between the middle value of E' in the first heating scan and in the cooling scan; $E'_{rel,-40^\circ\text{C}}$ = ratio between the value of E' at -40°C in the second heating scan and the first heating scan; $T_{h_1/c/h_2,\tan\delta} = \tan\delta$ peak temperature in the first heating (h_1), cooling (c) and second heating (h_2) scans

The same observations can be made also on the results of the cyclic DMA performed at 1 °C/min, reported in Fig. 9(c)–(d): E' is almost completely recovered on cooling (90–95%) and the crystallization is delayed with respect to the melting, but the hysteresis cycle of E' is narrower, as $\Delta T_{E'/50\%}$ is approx. 10 °C and the difference between the $\tan\delta$ peak positions on heating and on cooling is 12–14 °C (the same is true for E'' peaks).

The laminates were also subjected to multifrequency scans to investigate the effect of the frequency on the phase transition of the PCM and the glass transition of the matrix with the contemporary presence of the reinforcing fibers. The trends of the viscoelastic parameters of the samples EL-CF and EL-MC40-CF are reported in Fig. 10(a)–(b). For the neat laminate EL-CF, all the signals shift to higher temperatures with increasing frequency, but they show a strong dependency on the frequency only at the glass transition, unlike the neat EL resin, which further implies that the carbon fibers may hinder the low-temperature thermal transition observed on EL. The curves of sample EL-MC40-CF are qualitatively comparable to those of the matrix EL-MC40, as not only the E'' and $\tan\delta$ peaks related to T_g shift to higher temperatures with increasing frequency, but also those at the PCM phase change, and in this temperature range the frequency sensitivity is higher before than after the maximum. This is more clearly observable in Fig. 10(c), which shows the $\tan\delta$ peaks at the PCM melting for the four prepared laminates, compared to the DSC melting peak of the neat MC acquired at the same heating rate (0.3 °C/min). At this heating rate, the $\tan\delta$ maxima are found at lower temperature than the DSC peak. The $\tan\delta$ signals show a strong frequency dependence until the first steps of the melting phase change, but when the PCM is almost completely molten the frequency dependence weakens considerably. As for the matrices, the activation energy of the glass transition (E_a) was calculated from the $\tan\delta$ peaks. The results of the analysis with the linear regressions are shown in Fig. 10(d), while the E_a values are reported in Table 3. The values of E_a are generally slightly lower than those of the matrices, but, as for the samples EL-MC x ($x = 20, 30, 40$), E_a is not considerably affected by the MC concentration. As the melting E'' and $\tan\delta$ peaks also appear to depend on frequency, an attempt was made to check the suitability of the Arrhenius approach to calculate the activation energy of this transition. The results of this attempt are reported in Fig. 11. It can be seen that if a linear correlation can be estimated for the four lower frequency points, the last point deviates markedly from this trend, especially in the $\tan\delta$ peaks, thereby making

Fig. 10 Results on the DMA multifrequency scans on the samples EL-CF and EL-MC x -CF ($x = 20, 30, 40$). Investigated frequencies were 0.3, 1, 3, 10, and 30 Hz: **(a)** sample EL-CF; **(b)** sample EL-MC40-CF; **(c)** trend of $\tan \delta$ in the multifrequency scans for the samples EL-CF and EL-MC x -CF ($x = 20, 30, 40$), showing the peak of the melting process of the PCM, compared with a DSC scan on the PCM performed at the same scanning speed; **(d)** natural logarithm of the frequency ($\ln(\nu)$) as a function of $1000/T$ (peaks of $\tan \delta$ corresponding to the glass transition) for the samples EL-CF and EL-MC x -CF ($x = 20, 30, 40$)

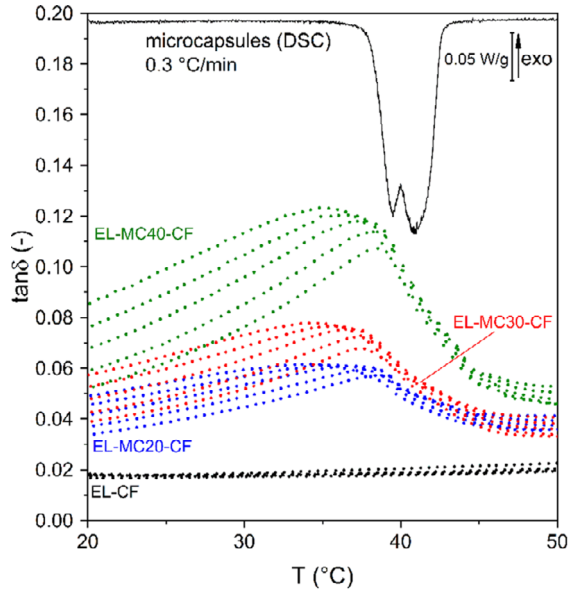


the application of a precise linear regression unfeasible. However, this DMA investigation allowed a better understanding of how the viscoelastic parameters of the structural TES composites vary as a function of temperature and frequency, thus providing an interesting insight on the use of DMA to study a melting phase transition and its effects on the dynamic-mechanical properties of the host laminate.

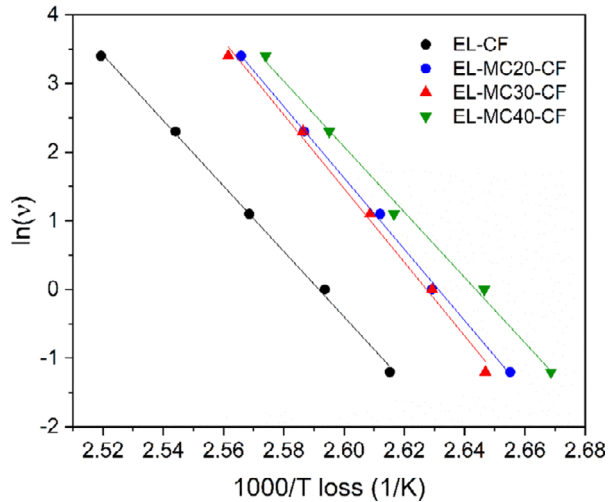
4 Conclusions

This work presented the results of a systematic dynamic-mechanical characterization of Elium[®]/PCM matrices and Elium[®]/PCM/carbon fiber laminates, performed by combining different testing modes, i.e., single frequency, cyclic (heating/cooling) and multifrequency scans. Single frequency scans on the samples EL-MC x ($x = 20, 30, 40$) evidenced the PCM melting as a decreasing step in E' and peaks in E'' and $\tan \delta$, while the T_g peaks of the acrylic matrix are visible at 100–120 °C, in agreement with DSC results. Multifrequency scans highlighted a strong dependency of E' on the applied frequency throughout the whole temperature range, and they pointed out that the not only the T_g peaks but also the melting peaks shifted to higher temperatures with increasing frequency. Similarly, the storage modulus of the laminates decreased in two main steps and E'' and $\tan \delta$ show asymmetric peaks in correspondence of the PCM melting and the resin glass transition. At the PCM

Fig. 10 (Continued)



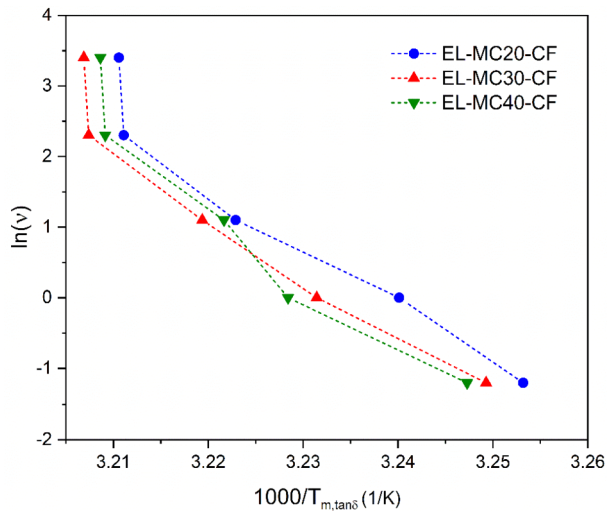
(c)



(d)

melting, the amplitude of the E' step and the intensity of the $\tan\delta$ peak showed a linear correlation with the MC weight fraction and the melting enthalpy, which points out a new interesting approach to compare two powerful techniques such as DSC and DMA to study the thermally activated transitions. Cyclic DMA showed that the decrease in E' during PCM melting is almost completely recovered (90–95%) upon crystallization, and the measured difference between the melting and crystallization points (supercooling) decreases with decreasing heating/cooling rate. As for the matrices, multifrequency DMA tests allowed the measurement of the activation energy of the glass transition, which appeared not to be affected by the PCM fraction. The peaks related to PCM melting are also affected by the

Fig. 11 Natural logarithm of the frequency ($\ln(\nu)$) as a function of $1000/T$ (peaks of $\tan \delta$ at the paraffin melting) for the samples EL-CF and EL-MC $_x$ -CF ($x = 20, 30, 40$)



applied frequency, and this is true mostly before than after the peak maximum, when the melting process is only partially complete. As also the position of this peaks changes with frequency, an attempt to apply the Arrhenius approach to these peaks was made, but the strong nonlinearity of the correlation prevented a precise application of the linear regression. This work contributed to shed light on how the dynamic-mechanical properties of polymers and laminates are affected by the presence of a PCM and by its phase change, which is extremely important for composites designed to combine the structural and TES functions. It also experimented the uncommon use of DMA to study a melting/crystallization phase change and found noteworthy correlations between DMA and DSC parameters.

Publisher's Note Springer Nature remains neutral with regard to jurisdictional claims in published maps and institutional affiliations.

References

- Abhat, A.: Low temperature latent heat thermal energy storage: heat storage materials. *Sol. Energy* **30**(4), 313–332 (1983)
- Bagotia, N., Sharma, D.K.: Systematic study of dynamic mechanical and thermal properties of multiwalled carbon nanotube reinforced polycarbonate/ethylene methyl acrylate nanocomposites. *Polym. Test.* **73**, 425–432 (2019). <https://doi.org/10.1016/j.polymertesting.2018.12.006>
- Bayés-García, L., Ventolà, L., Cordobilla, R., Benages, R., Calvet, T., Cuevas-Diarte, M.A.: Phase change materials (PCM) microcapsules with different shell compositions: preparation, characterization and thermal stability. *Sol. Energy Mater. Sol. Cells* **94**(7), 1235–1240 (2010). <https://doi.org/10.1016/j.solmat.2010.03.014>
- Bhudolia, S.K., Perrotey, P., Joshi, S.C.: Enhanced vibration damping and dynamic mechanical characteristics of composites with novel pseudo-thermoset matrix system. *Compos. Struct.* **179**, 502–513 (2017). <https://doi.org/10.1016/j.compstruct.2017.07.093>
- Cao, L., Tang, F., Fang, G.: Synthesis and characterization of microencapsulated paraffin with titanium dioxide shell as shape-stabilized thermal energy storage materials in buildings. *Energy Build.* **72**, 31–37 (2014). <https://doi.org/10.1016/j.enbuild.2013.12.028>
- Chartoff, R.P., Menczel, J.D., Dillman, S.H.: Dynamic mechanical analysis (DMA). In: Menczel, J.D., Prime, R.B. (eds.) *Thermal Analysis of Polymers. Fundamentals and Applications*. Wiley, Hoboken (2009), Chap. 5

- Chee, S.S., Jawaid, M., Sultan, M.T.H., Alothman, O.Y., Abdullah, L.C.: Thermomechanical and dynamic mechanical properties of bamboo/woven kenaf mat reinforced epoxy hybrid composites. *Composites Part B. Engineering* **163**, 165–174 (2019). <https://doi.org/10.1016/j.compositesb.2018.11.039>
- Chen, Z., Cao, L., Shan, F., Fang, G.: Preparation and characteristics of microencapsulated stearic acid as composite thermal energy storage material in buildings. *Energy Build.* **62**, 469–474 (2013). <https://doi.org/10.1016/j.enbuild.2013.03.025>
- Clarke, R.L., Braden, M.: Modified Arrhenius equation for the frequency dependence of the transition temperatures of polymers. *Biomaterials* **10**, 349–352 (1989)
- Devi, L.U., Bhagawan, S.S., Thomas, S.: Dynamic mechanical analysis of pineapple leaf/glass hybrid fiber reinforced polyester composites. In: *Polymer Composites, NA-NA* (2009). <https://doi.org/10.1002/pc.20880>
- Dirand, M., Bouroukba, M., Chevallier, V., Petitjean, D.: Normal alkanes, multialkane synthetic model mixtures, and real petroleum waxes: crystallographic structures, thermodynamic properties, and crystallization. *J. Chem. Eng. Data* **47**, 115–143 (2002). <https://doi.org/10.1021/je0100084>
- Dorigato, A., Canclini, P., Unterberger, S.H., Pegoretti, A.: Phase changing nanocomposites for low temperature thermal energy storage and release. *eXPRESS Polym. Lett.* **11**(9), 738–752 (2017a). <https://doi.org/10.3144/expresspolymlett.2017.71>
- Dorigato, A., Ciampolillo, M.V., Cataldi, A., Bersani, M., Pegoretti, A.: Polyethylene wax/EPDM blends as shape-stabilized phase change materials for thermal energy storage. *Rubber Chem. Technol.* **90**(3), 575–584 (2017b). <https://doi.org/10.5254/rct.82.83719>
- Dorigato, A., Fredi, G., Pegoretti, A.: Novel phase change materials using thermoplastic composites. In: 9th International Conference on “Times of Polymers and Composites”. AIP Conference Proceedings, vol. 1981, pp. 020044/020041–020044/020044 (2018). <https://doi.org/10.1063/1.5045906>
- Dorigato, A., Fredi, G., Pegoretti, A.: Application of the thermal energy storage concept to novel epoxy/short carbon fiber composites. *J. Appl. Polym. Sci.* **136**(21), 47434/47431–47434/47439 (2019). <https://doi.org/10.1002/app.47434>
- Fambri, L., Kesenci, K., Migliaresi, C.: Characterization of modulus and glass transition phenomena in poly(L-lactide)/hydroxyapatite composites. *Polym. Compos.* **24**(1), 100–108 (2003)
- Fang, X., Fan, L.W., Ding, Q., Yao, X.L., Wu, Y.Y., Hou, J.F., Wang, X., Yu, Z.T., Cheng, G.H., Hu, Y.C.: Thermal energy storage performance of paraffin-based composite phase change materials filled with hexagonal boron nitride nanosheets. *Energy Convers. Manag.* **80**, 103–109 (2014). <https://doi.org/10.1016/j.enconman.2014.01.016>
- Flores, R., Perez, J., Cassagnau, P., Michel, A., Cavaille, J.Y.: Dynamic mechanical behavior of poly(vinyl chloride)/poly(methyl methacrylate) polymer blend. *J. Appl. Polym. Sci.* **60**, 1439–1453 (1996)
- Fredi, G., Dorigato, A., Fambri, L., Pegoretti, A.: Wax confinement with carbon nanotubes for phase changing epoxy blends. *Polymers* **9**(9), 405/401–405/416 (2017). <https://doi.org/10.3390/polym9090405>
- Fredi, G., Dorigato, A., Fambri, L., Pegoretti, A.: Multifunctional epoxy/carbon fiber laminates for thermal energy storage and release. *Compos. Sci. Technol.* **158**, 101–111 (2018a). <https://doi.org/10.1016/j.compscitech.2018.02.005>
- Fredi, G., Dorigato, A., Pegoretti, A.: Multifunctional glass fiber/polyamide composites with thermal energy storage/release capability. *eXPRESS Polym. Lett.* **12**, 349–364 (2018b). <https://doi.org/10.3144/expresspolymlett.2018.30>
- Fredi, G., Dorigato, A., Pegoretti, A.: Novel reactive thermoplastic resin as a matrix for laminates containing phase change microcapsules. *Polym. Compos.* **40**(9), 3711–3724 (2019a). <https://doi.org/10.1002/pc.25233>
- Fredi, G., Dorigato, A., Unterberger, S., Artuso, N., Pegoretti, A.: Discontinuous carbon fiber/polyamide composites with microencapsulated paraffin for thermal energy storage. *J. Appl. Polym. Sci.* **136**(16), 47408/47401–47408/47414 (2019b). <https://doi.org/10.1002/app.47408>
- Gamon, G., Evon, P., Rigal, L.: Twin-screw extrusion impact on natural fibre morphology and material properties in poly(lactic acid) based biocomposites. *Ind. Crop. Prod.* **46**, 173–185 (2013). <https://doi.org/10.1016/j.indcrop.2013.01.026>
- Goertzen, W.K., Kessler, M.R.: Dynamic mechanical analysis of carbon/epoxy composites for structural pipeline repair. *Composites Part B. Engineering* **38**(1), 1–9 (2007). <https://doi.org/10.1016/j.compositesb.2006.06.002>
- Hu, J., Zhang, X., Qu, J., Wen, Y., Sun, W.: Synthesis, characterizations and mechanical properties of microcapsules with dual shell of polyurethane (PU)-melamine formaldehyde (MF): effect of different chain extenders. *Ind. Eng. Chem. Res.* (2018). <https://doi.org/10.1021/acs.iecr.7b04973>
- Jaguemont, J., Omar, N., Van den Bossche, P., Mierlo, J.: Phase-change materials (PCM) for automotive applications: a review. *Appl. Therm. Eng.* **132**, 308–320 (2018). <https://doi.org/10.1016/j.applthermaleng.2017.12.097>

- Jeong, S.-G., Kim, S., Huh, W.: Preparation of epoxy resin using n-hexadecane based shape stabilized PCM for applying wood-based flooring. *J. Adhes. Sci. Technol.* **28**(7), 711–721 (2014). <https://doi.org/10.1080/01694243.2013.865331>
- Kahwaji, S., Johnson, M.B., Kheirabadi, A.C., Groulx, D., White, M.A.: A comprehensive study of properties of paraffin phase change materials for solar thermal energy storage and thermal management applications. *Energy* **162**, 1169–1182 (2018). <https://doi.org/10.1016/j.energy.2018.08.068>
- Karbhari, V.M., Wang, Q.: Multi-frequency dynamic mechanical thermal analysis of moisture uptake in E-glass/vinylester composites. *Composites Part B. Engineering* **35**(4), 299–304 (2004). <https://doi.org/10.1016/j.compositesb.2004.01.003>
- Keller, M.W., Jellison, B.D., Ellison, T.: Moisture effects on the thermal and creep performance of carbon fiber/epoxy composites for structural pipeline repair. *Composites Part B. Engineering* **45**(1), 1173–1180 (2013). <https://doi.org/10.1016/j.compositesb.2012.07.046>
- Kenisarin, M., Mahkamov, K.: Solar energy storage using phase change materials. *Renew. Sustain. Energy Rev.* **11**(9), 1913–1965 (2007). <https://doi.org/10.1016/j.rser.2006.05.005>
- Kenisarin, M.M., Kenisarina, K.M.: Form-stable phase change materials for thermal energy storage. *Renew. Sustain. Energy Rev.* **16**(4), 1999–2040 (2012). <https://doi.org/10.1016/j.rser.2012.01.015>
- Krupa, I., Míková, G., Luyt, A.S.: Polypropylene as a potential matrix for the creation of shape stabilized phase change materials. *Eur. Polym. J.* **43**(3), 895–907 (2007). <https://doi.org/10.1016/j.eurpolymj.2006.12.019>
- Krupa, I., Nógellová, Z., Špitalský, Z., Janigová, I., Boh, B., Sumiga, B., Kleinová, A., Karkri, M., Al-Maadeed, M.A.: Phase change materials based on high-density polyethylene filled with microencapsulated paraffin wax. *Energy Convers. Manag.* **87**, 400–409 (2014). <https://doi.org/10.1016/j.enconman.2014.06.061>
- Li, G., Lee-Sullivan, P., Thring, R.W.: Determination of activation energy for glass transition of an epoxy adhesive using dynamic mechanical analysis. *J. Therm. Anal. Calorim.* **60**, 377–390 (2000)
- Lian, Q., Li, K., Sayyed, A.A.S., Cheng, J., Zhang, J.: Study on a reliable epoxy-based phase change material: facile preparation, tunable properties, and phase/microphase separation behavior. *Mater. Chem. A* **5**, 14562–14574 (2017). <https://doi.org/10.1039/C7TA02816D>
- Liu, X., Lou, Y.: Preparation of microencapsulated phase change materials by the sol-gel process and its application on textiles. *Fibres Text. East. Eur.* **23**(2), 63–67 (2015)
- Luyt, A.S., Krupa, I.: Phase change materials formed by UV curable epoxy matrix and Fischer-Tropsch paraffin wax. *Energy Convers. Manag.* **50**(1), 57–61 (2009). <https://doi.org/10.1016/j.enconman.2008.08.026>
- Lv, Y., Li, A., Zhou, F., Pan, X., Liang, F., Qu, X., Qiu, D., Yang, Z.: A novel composite PMMA-based bone cement with reduced potential for thermal necrosis. *ACS Appl. Mater. Interfaces* **7**(21), 11280–11285 (2015). <https://doi.org/10.1021/acsami.5b01447>
- Menard, K.P.: Dynamic testing and instrumentation. In: Menard, K.P. (ed.) *Dynamic Mechanical Analysis. A Practical Introduction*. CRC Press, Boca Raton (2008), Chap. 5
- Mngomezulu, M.E., Luyt, A.S., Krupa, I.: Structure and properties of phase change materials based on HDPE, soft Fischer-Tropsch paraffin wax, and wood flour. *J. Appl. Polym. Sci.* **118**(3), 1541–1551 (2010). <https://doi.org/10.1002/app.32521>
- Mochane, M.J., Luyt, A.S.: Preparation and properties of polystyrene encapsulated paraffin wax as possible phase change material in a polypropylene matrix. *Thermochim. Acta* **544**(Suppl. C), 63–70 (2012). <https://doi.org/10.1016/j.tca.2012.06.017>
- Peng, H., Zhang, D., Ling, X., Li, Y., Wang, Y., Yu, Q., She, X., Li, Y., Ding, Y.: n-Alkanes phase change materials and their microencapsulation for thermal energy storage: a critical review. *Energy Fuels* **32**(7), 7262–7293 (2018). <https://doi.org/10.1021/acs.energyfuels.8b01347>
- Pereira da Cunha, J., Eames, P.: Thermal energy storage for low and medium temperature applications using phase change materials—a review. *Appl. Energy* **177**, 227–238 (2016). <https://doi.org/10.1016/j.apenergy.2016.05.097>
- Pielichowska, K., Pielichowski, K.: Phase change materials for thermal energy storage. *Prog. Mater. Sci.* **65**, 67–123 (2014). <https://doi.org/10.1016/j.pmatsci.2014.03.005>
- Popelka, A., Sobolčák, P., Mrlík, M., Nógellova, Z., Chodák, I., Ouederni, M., Al-Maadeed, M.A., Krupa, I.: Foamy phase change materials based on linear low-density polyethylene and paraffin wax blends. *Emerg. Mater.* **1**(1–2), 47–54 (2018). <https://doi.org/10.1007/s42247-018-0003-3>
- Rigotti, D., Dorigato, A., Pegoretti, A.: 3D printable thermoplastic polyurethane blends with thermal energy storage/release capabilities. *Mater. Today Commun.* **15**, 228–235 (2018). <https://doi.org/10.1016/j.mtcomm.2018.03.009>
- Sarier, N., Onder, E.: Thermal characteristics of polyurethane foams incorporated with phase change materials. *Thermochim. Acta* **454**(2), 90–98 (2007). <https://doi.org/10.1016/j.tca.2006.12.024>

- Sharma, R.K., Ganesan, P., Tyagi, V.V., Metselaar, H.S.C., Sandaran, S.C.: Developments in organic solid–liquid phase change materials and their applications in thermal energy storage. *Energy Convers. Manag.* **95**, 193–228 (2015). <https://doi.org/10.1016/j.enconman.2015.01.084>
- Shin, J.H., Kim, D., Centea, T., Nutt, S.R.: Thermoplastic prepreg with partially polymerized matrix: material and process development for efficient part manufacturing. *Composites, Part A, Appl. Sci. Manuf.* **119**, 154–164 (2019). <https://doi.org/10.1016/j.compositesa.2019.01.009>
- Sobolciak, P., Karkri, M., Al-Maaded, M.A., Krupa, I.: Thermal characterization of phase change materials based on linear low-density polyethylene, paraffin wax and expanded graphite. *Renew. Energy* **88**, 372–382 (2016). <https://doi.org/10.1016/j.renene.2015.11.056>
- Sobolciak, P., Mrlík, M., AlMaadeed, M.A., Krupa, I.: Calorimetric and dynamic mechanical behavior of phase change materials based on paraffin wax supported by expanded graphite. *Thermochim. Acta* **617**, 111–119 (2015). <https://doi.org/10.1016/j.tca.2015.08.026>
- Su, J.-F., Wang, X.-Y., Wang, S.-B., Zhao, Y.-H., Zhu, K.-Y., Yuan, X.-Y.: Interface stability behaviors of methanol-melamine-formaldehyde shell microPCMs/epoxy matrix composites. *Polym. Compos.* **32**(5), 810–820 (2011). <https://doi.org/10.1002/pc.21102>
- Su, J.F., Zhao, Y.H., Wang, X.Y., Dong, H., Wang, S.B.: Effect of interface debonding on the thermal conductivity of microencapsulated-paraffin filled epoxy matrix composites. *Composites, Part A, Appl. Sci. Manuf.* **43**(3), 325–332 (2012). <https://doi.org/10.1016/j.compositesa.2011.12.003>
- Sun, Y., Zhang, Z., Moon, K.-S., Wong, C.P.: Glass transition and relaxation behavior of epoxy nanocomposites. *J. Polym. Sci., Part B, Polym. Phys.* **42**(21), 3849–3858 (2004). <https://doi.org/10.1002/polb.20251>
- Sundararajan, S., Kumar, A., Chakraborty, B.C., Samui, A.B., Kulkarni, P.S.: Poly(ethylene glycol) (PEG)-modified epoxy phase-change polymer with dual properties of thermal storage and vibration damping. *Sustain. Energy Fuels* **2**(3), 688–697 (2018). <https://doi.org/10.1039/c7se00552k>
- Vélez, C., Khayet, M., Ortiz de Zárate, J.M.: Temperature-dependent thermal properties of solid/liquid phase change even-numbered n-alkanes: n-hexadecane, n-octadecane and n-eicosane. *Appl. Energy* **143**, 383–394 (2015). <https://doi.org/10.1016/j.apenergy.2015.01.054>
- Wang, F., Lin, W., Ling, Z., Fang, X.: A comprehensive review on phase change material emulsions: fabrication, characteristics, and heat transfer performance. *Sol. Energy Mater. Sol. Cells* **191**, 218–234 (2019). <https://doi.org/10.1016/j.solmat.2018.11.016>
- Wang, S., Tozaki, K.-i., Hayashi, H., Hosaka, S., Inaba, H.: Observation of multiple phase transitions in n-C₂₂H₄₆ using a high resolution and super-sensitive DSC. *Thermochim. Acta* **408**(1–2), 31–38 (2003). [https://doi.org/10.1016/s0040-6031\(03\)00312-5](https://doi.org/10.1016/s0040-6031(03)00312-5)
- Wang, X.-Y., Su, J.-F., Wang, S.-B., Zhao, Y.-H.: The effect of interface debonding behaviors on the mechanical properties of microPCMs/epoxy composites. *Polym. Compos.* **32**(9), 1439–1450 (2011). <https://doi.org/10.1002/pc.21174>
- Wirtz, R., Fuchs, A., Narla, V., Shen, Y., Zhao, T., Jiang, Y.: In: *A Multi-Functional Graphite/Epoxy-Based Thermal Energy Storage Composite for Temperature Control of Sensors and Electronics*, University of Nevada, Reno, Nevada, 89557 USA, 2003, 2003, pp. 1–9
- Yoo, S., Kandare, E., Mahendrarajah, G., Al-Maadeed, M.A., Khatibi, A.A.: Mechanical and thermal characterisation of multifunctional composites incorporating phase change materials. *J. Compos. Mater.* **51**(18), 2631–2642 (2017a). <https://doi.org/10.1177/0021998316673894>
- Yoo, S., Kandare, E., Shanks, R., Al-Maadeed, M.A., Afaghi Khatibi, A.: Thermophysical properties of multifunctional glass fibre reinforced polymer composites incorporating phase change materials. *Thermochim. Acta* **642**, 25–31 (2016). <https://doi.org/10.1016/j.tca.2016.09.003>
- Yoo, S., Kandare, E., Shanks, R., Khatibi, A.A.: *Viscoelastic Characterization of Multifunctional Composites Incorporated with Microencapsulated Phase Change Materials*. International Conference of Materials Processing and Characterization (ICPMC). Elsevier, Amsterdam (2017b)
- Yung, K., Zhu, B., Yue, T., Xie, C.: Preparation and properties of hollow glass microsphere-filled epoxy-matrix composites. *Compos. Sci. Technol.* **69**(2), 260–264 (2009). <https://doi.org/10.1016/j.compscitech.2008.10.014>
- Zalba, B., Marin, J.M., Cabeza, L.F., Mehling, H.: Review on thermal energy storage with phase change: materials, heat transfer analysis and applications. *Appl. Therm. Eng.* **23**, 251–283 (2003). [https://doi.org/10.1016/S1359-4311\(02\)00192-8](https://doi.org/10.1016/S1359-4311(02)00192-8)
- Zhang, H., Baeyens, J., Cáceres, G., Degrève, J., Lv, Y.: Thermal energy storage: recent developments and practical aspects. *Prog. Energy Combust. Sci.* **53**, 1–40 (2016). <https://doi.org/10.1016/j.peccs.2015.10.003>
- Zhang, P., Hu, Y., Song, L., Ni, J., Xing, W., Wang, J.: Effect of expanded graphite on properties of high-density polyethylene/paraffin composite with intumescent flame retardant as a shape-stabilized phase change material. *Sol. Energy Mater. Sol. Cells* **94**(2), 360–365 (2010). <https://doi.org/10.1016/j.solmat.2009.10.014>